BBA - Bioenergetics 1860 (2019) 148061

Contents lists available at ScienceDirect

BBA - Bioenergetics

journal homepage: www.elsevier.com/locate/bbabio

Functional analysis of coiled-coil domains of MCU in mitochondrial calcium uptake

Takenori Yamamoto[a,b,*], Mizune Ozono[a,b], Akira Watanabe[a,b], Kosuke Maeda[a,b], Atsushi Nara[a,b], Mei Hashida[a,b], Yusuke Ido[a,b], Yuka Hiroshima[a], Akiko Yamada[c], Hiroshi Terada[d], Yasuo Shinohara[a,b,*]

[a] Institute for Genome Research, Tokushima University, Kuramotocho-3, Tokushima 770-8503, Japan
[b] Faculty of Pharmaceutical Sciences, Tokushima University, Shomachi-1, Tokushima 770-8505, Japan
[c] School of Dentistry, Tokushima University, Kuramotocho-3, Tokushima 770-8504, Japan
[d] Niigata University of Pharmacy and Applied Life Sciences, Niigata City 956-8603, Japan

ARTICLE INFO

Keywords:
Calcium uniporter
Coiled coil
Ion channel
MCU
Mitochondria
Yeast

ABSTRACT

The mitochondrial calcium uniporter (MCU) complex is a highly-selective calcium channel. This complex consists of MCU, mitochondrial calcium uptake proteins (MICUs), MCU regulator 1 (MCUR1), essential MCU regulator element (EMRE), etc. MCU, which is the pore-forming subunit, has 2 highly conserved coiled-coil domains (CC1 and CC2); however, their functional roles are unknown. The yeast expression system of mammalian MCU and EMRE enables precise reconstitution of the properties of the mammalian MCU complex in yeast mitochondria. Using the yeast expression system, we here showed that, when MCU mutant lacking CC1 or CC2 was expressed together with EMRE in yeast, their mitochondrial Ca^{2+}-uptake function was lost. Additionally, point mutations in CC1 or CC2, which were expected to prevent the formation of the coiled coil, also disrupted the Ca^{2+}-uptake function. Thus, it is essential for the Ca^{2+} uptake function of MCU that the coiled-coil structure be formed in CC1 and CC2. The loss of function of those mutated MCUs was also observed in the mitochondria of a yeast strain lacking the yeast MCUR1 homolog. Also, in the *D. discoideum* MCU, which has EMRE-independent Ca^{2+}-uptake function, the deletion of either CC1 or CC2 caused the loss of function. These results indicated that the critical functions of CC1 and CC2 were independent of other regulatory subunits such as MCUR1 and EMRE, suggesting that CC1 and CC2 might be essential for pore formation by MCUs themselves. Based on the tetrameric structure of MCU, we discussed the functional roles of the coiled-coil domains of MCU.

1. Introduction

Mitochondrial calcium homeostasis plays critical roles in cell survival and aerobic metabolism in eukaryotes [1–3]. Moreover, excessive Ca^{2+} accumulation in mitochondria renders their inner membrane permeable. This phenomenon is referred to as the permeability transition, resulting in apoptosis and necrosis [4–6]; and these processes are related to various kinds of diseases [7,8]. The mitochondrial calcium uniporter is a highly selective ion channel that guarantees Ca^{2+} accumulation inside the mitochondrial matrix [9–11]. In this decade, the molecular composition of this calcium-uptake complex was revealed to consist of the following: the mitochondrial calcium uniporter (MCU) [12,13], mitochondrial calcium uptake proteins 1, 2, 3 (MICU1, MICU2, MICU3) [14,15], mitochondrial calcium uniporter regulator 1 (MCUR1) [16], an MCU isoform (MCUb) [17], and the essential MCU regulator (EMRE) [18]. The MCU possesses 2 transmembrane regions, and the MCU oligomer forms a pore [12,13]. MICU isoforms cooperatively function as regulators of Ca^{2+} uptake by the MCU oligomer [19–21]; and MICU1 also contributes to the apparent ion selectivity [22]. MCUR1 is considered to be necessary for regulation of the Ca^{2+} threshold as well as for the stability of the MCU, EMRE-oligomer [23,24]. In mammalian mitochondria, the EMRE is an essential factor for Ca^{2+} uptake by MCU [18,25,26], but its functional roles in this uptake are not yet sufficiently understood.

The MCU has a widely conserved domain organization [27]. MCU has a mitochondrial targeting signal (MTS) at its N terminus, which is

Abbreviations: CC, coiled-coil region; EGFP, enhanced green fluorescent protein; EM, electron microscopy; EMRE, essential MCU regulator; MCU, mitochondrial calcium uniporter; MCUR1, mitochondrial calcium uniporter regulator 1; MICU1, mitochondrial calcium uptake protein 1; MTS, mitochondrion-targeting signal

* Corresponding authors at: Institute for Genome Research, Tokushima University, Kuramotocho-3, Tokushima 770-8503, Japan.
E-mail addresses: tyamamo@genome.tokushima-u.ac.jp (T. Yamamoto), yshinoha@genome.tokushima-u.ac.jp (Y. Shinohara).

https://doi.org/10.1016/j.bbabio.2019.148061
Received 12 February 2019; Received in revised form 20 July 2019; Accepted 2 August 2019
Available online 05 August 2019

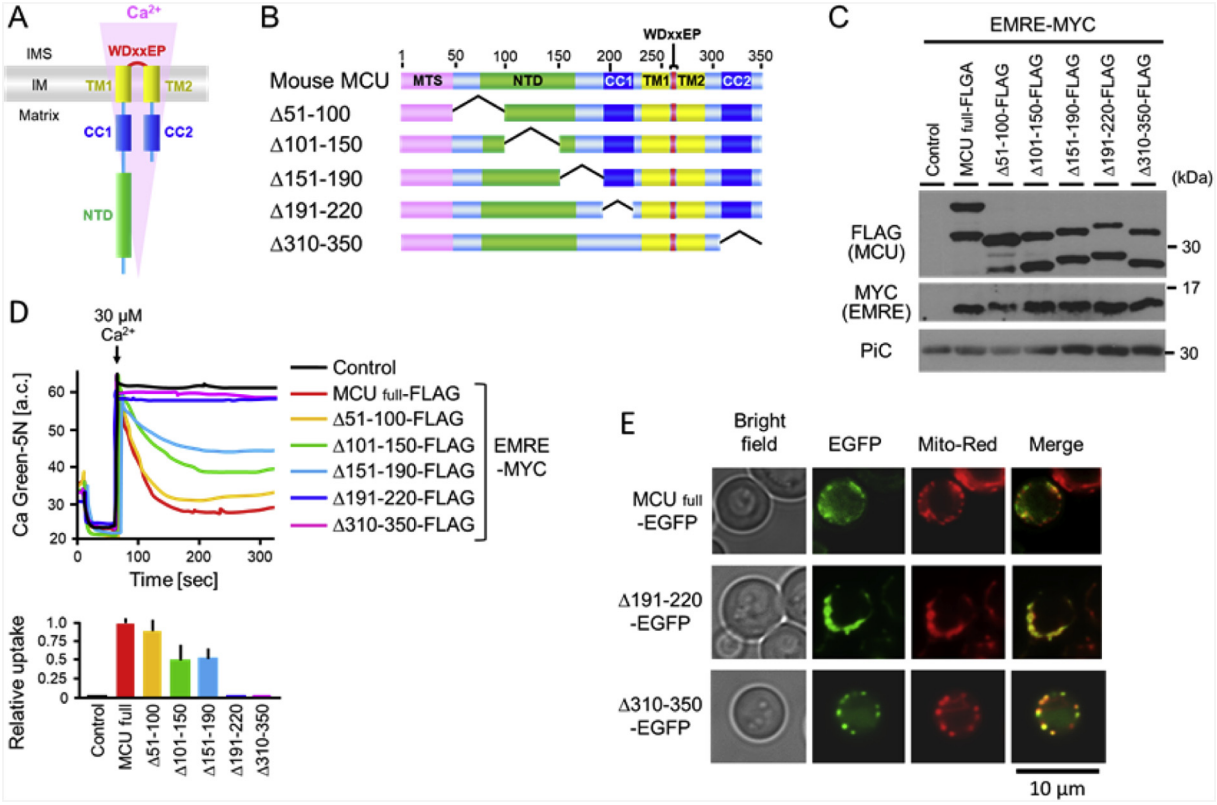

Fig. 1. Identification of amino acid regions in mouse MCU critical for Ca^{2+} uptake. (A), Domains/motifs in and topology of the mitochondrial inner membrane (IM) of mouse MCU. NTD, N-terminal domain; CC, coiled-coil domain; TM, transmembrane region. (B), Schematic representation of full-length MCU and its deletion mutants, showing predicted domains and motif: the mitochondrial translocation signal (MTS) at Met1-Thr49; NTD at Val74-Arg164; CC1 and CC2 at Ile191-Arg220 and Arg310-Gln338, respectively; TM1 and TM2 at Leu233-Glu256 and Val265-Val282, respectively; and WDxxEP motif at Trp259-Pro264. (C), Immunoblots of mitochondria isolated from yeast expressing the above-indicated FLAG-tagged MCU deletion mutants together with MYC-tagged EMRE. The mitochondrial phosphate carrier (PiC) was used as a loading control for mitochondria. (D), Mitochondrial Ca^{2+} uptake. Upper: representative traces of calcium uptake by mitochondria from the transformants having the indicated proteins, with 30 μM $CaCl_2$ added at the time indicated by the arrow. Lower: Relative rates of Ca^{2+} uptake defined as the change in luminescence at 150 s, normalized by the uptake in the mitochondria bearing MCU_{full}-FLAG and EMRE-MYC (mean ± s.d.); n ≥ 3. (E), Intracellular localization of the indicated proteins fused with EGFP, with MitoTracker Red used as a mitochondrial marker.

followed by an N-terminal domain (NTD); whereas, the C-terminal region of MCU has 2 transmembrane regions (TM1 and TM2), 2 coiled-coil motifs (CC1 and CC2), and a highly conserved WDxxEP motif located between TM1 and TM2 (Fig. 1A). The WDxxEP motif is located in the inter membrane space (IMS) side of the mitochondrial inner membrane (IM) [28]. Aspartate and glutamate residues in this motif are critical for Ca^{2+} uptake, indicating that this motif forms a Ca^{2+}-selective filter [12,13]. Up until now, various 3D structures of the MCU have been reported. First, Lee et al. revealed the X-ray crystal structure of the NTD of human MCU, and they showed that the phosphorylation of a serine residue in the NTD activated the mitochondrial Ca^{2+} uptake function [29]. After that, by using NMR and Cryo-EM Oxenoid et al. showed the structure of *Caenorhabditis elegans* MCU lacking NTD; and in their structure model, the MCUs formed a pentamer [30]. Recently, 4 independent groups showed the structure of MCUs including the NTD in fungi and zebrafish; and their MCU structures were tetrameric, not pentameric [31–34]. The structures of some of the functional domains in MCU tetramer models were also different from those of the MCU pentamer model. The combination of the 3D structures of MCU and the findings from past biological mutation studies allow us to understand how the WDxxEP motif forms the pore entrance and how this motif functions as a Ca^{2+}-selective filter. On the other hand, the roles of the regions other than the WDxxEP motif of MCU in Ca^{2+} uptake function are not yet adequately understood. Therefore, after Ca^{2+} is selectively filtered at the WDxxEP motif located in the inter membrane space side, how the Ca^{2+} is transported into the matrix through the domains located in the inner membrane and those in the matrix is unknown.

Although MCU complexes are conserved over a wide range of species, the yeast *S. cerevisiae* has no orthologues of the subunits of the mammalian MCU complex [27]; and, actually, yeast mitochondria completely lack Ca^{2+} uptake activity [35,36]. Therefore, a yeast expression system easily allows the production of yeast mitochondria expressing specific subunits of the mammalian MCU complex; and by using such mitochondria, their structures and functions can be analyzed [25,37]. We previously established a yeast expression system for the native-form mouse MCU; and this expression system enabled us to precisely reconstitute the properties of the mammalian MCU complex in yeast mitochondria [26]. Using this system, in the present study, we analyzed the structure-function relationships of various regions of the mouse MCU.

2. Materials and methods

2.1. Materials

Yeast strain W303-1B (*MATα, ade2-1, his3-11,15, leu2-3,112, ura3-1, trp1-1, can1-100*) was supplied by Dr. Shigeomi Shimizu; and the yeast shuttle vector pYO326 (multi-copy vector, reported as pSQ326 [38]), by Dr. Akihiko Nakano. Anti-FLAG antibody (code F7425-2MG) and anti-MYC antibody (code 2276S) were both obtained from Sigma-Aldrich Japan (Osaka, JP). Calcium Green-5N was purchased from Molecular Probes (Eugene, OR, USA).

2.2. Preparation of expression vectors and yeast transformants

To prepare the expression vectors, we used pYO326/*TDH*p (*URA3* [or *LEU2*]), which is a multicopy vector with a glyceraldehyde-3-phosphate dehydrogenase (*TDH*) promoter and *URA3* (or *LEU2*) as a selection marker gene [26]. The codon-optimized mouse MCU, which was synthesized as described in our previous report [26], was used as a template of MCU. The cDNA of *D. discoideum* MCU (DdMCU) was artificially synthesized based on the published protein sequence (UniProt ID: Q54LT0). FLAG-tagged MCU, EGFP-tagged MCU, and MYC-tagged EMRE, all tagged at their C-terminus, were inserted into the *Nde*I site and BamHI site of pYO326/*TDH*p (*URA3*) and pYO326/*TDH*p (*LEU2*), respectively. Deletion mutants and point mutants of MCU were prepared by PCR using each primer set shown in Supplemental Table SI. The PCR products were inserted into the *Nde* I site and BamHI site of pYO326/*TDH*p(*URA3*). Wild-type yeast was transformed by the plasmids by using the lithium acetate transformation method. Yeast cells were grown in SD medium without uracil or leucine for cells transformed with pYO326/*TDH*p(*URA3*) or pYO326/*TDH*p(*LEU2*), respectively. All recombinant DNA experiments were carried out according to the experimental guidelines of Tokushima University (approval number: 23-217).

2.3. Preparation of FMP32 deletion mutant

The targeting DNA for *FMP32* knock out was prepared by PCR using primer sets (Supplemental Table SI) and a selection marker gene *(HIS3* of pRS313) as a template. The targeting DNA was prepared by the fusion of 42,815–42,874 of chromosome VI (NC_001138.5) and nucleotide 43,379–43,438 to *HIS3* at its 5'terminus and 3′ terminus, respectively. Wild-type yeast in SD plates without histidine was transformed by the targeting DNA. To confirm the phenotype of the acquired *FMP32* KO strain, we incubated the yeast strain on YP medium containing 2% glucose or 3% glycerol at 37 °C.

2.4. Isolation of mitochondria from yeast cells

Yeast mitochondria were isolated as described in our previous work [39]. Briefly, the cells were precultured at 30 °C in SD medium (2% glucose, 6.7 g/L yeast nitrogen base without amino acids) containing supplements except for amino acids used as selection markers. After the preculture period, the cells (A_{600} = 2.0) were added to 1000 ml of YPGal medium (1% yeast extract, 2% bacto-polypeptone, and 2% galactose); and then incubation was carried out at 30 °C for 15 h. The cells were twice washed with cold water, after which they were incubated in 10 mM dithiothreitol (DTT) and 0.1 M Tris-SO_4 (pH 8.0) at 30 °C for 15 min. Next, they were incubated at 30 °C for 15 min with 11.39 mg of zymolyase 20 T in KPi medium (1.2 M sorbital, 20 mM potassium phosphate [pH 7.4], 2 mM EDTA) per g of cells to form spheroplasts. The spheroplasts were subsequently homogenized (5 strokes) in mannitol medium (0.6 M mannitol, 10 mM Tris-HCl [pH 7.4], 0.1% BSA, 2 mM EDTA, protease inhibitor cocktail) in a chilled Potter-Elvehjem homogenizer. Afterwards the homogenate was centrifuged for 5 min at 800 ×*g*, the supernatant was centrifuged for 10 min at 6800 ×*g*, and the resulting pellet was suspended in mannitol medium.

2.5. Measurement of calcium uptake

Isolated mitochondria (0.14 mg/ml) were incubated at 25 °C in incubation medium (0.3 M mannitol, 0.5 mg/ml BSA, 10 mM KPi, 2 mM NADH; pH 7.4 as a respiratory substrate) to which a calcium indicator (1 μM Calcium Green-5N) was added. Calcium ions in the reaction medium were measured by use of a Hitachi spectrofluorometer, model F-2700 (excitation = 506 nm, emission = 532 nm).

2.6. Imaging of EGFP-tagged MCU mutants in yeast cells

Imaging of MCU mutants in yeast cells was carried out by observing cells with EGFP-tagged MCU mutants and staining with MitoTracker Red (Invitrogen). Fluorescence observation was performed by using AMG fluorescence microscopy and an EVOS FL cell imaging system.

2.7. Immunodetection of proteins and preparation of antibody

Immunodetection of proteins was performed according to a previous report [40]. Antiserum against the mitochondrial phosphate carrier (PiC) was prepared from a rabbit that had been immunized with the synthetic peptide GMVGSFKQIIAGEGAGALLC, as described earlier [41].

3. Results

3.1. Identification of amino acid regions in mouse MCU critical for mitochondrial Ca^{2+} uptake

When an expression vector having the native nucleotide sequence of MCU is used to express mouse MCU in yeast, the protein level is very low; however, codon optimization of the N-terminal region of mouse MCU allows the protein level to become high, and the expression of this optimized MCU together with EMRE in yeast mitochondria enables reconstitution of the Ca^{2+} uptake function [26]. By use of the nucleotide sequence of the optimized mouse MCU for yeast as a template, we herein prepared various truncation mutants of MCU and examined the effects of the truncation on the Ca^{2+} uptake function. Mouse MCU has various functional motifs and domains: the mitochondrion-targeting signal (MTS) in Met1-Thr49, N-terminal domain (NTD) in Val74-Arg164, coiled-coil domains in Ile191-Arg220 (CC1) and Arg310-Gln338 (CC2), WDxxEP motif in Trp259-Pro264, and 2 transmembrane regions, one in Leu233-Glu256 (TM1) and the other in Val265-Val282 (TM2). Some previous reports showed that mutations in the WDxxEP motif cause loss of MCU function [12,13]. To identify the critical region (s) for the Ca^{2+} uptake activity other than the WDxxEP motif, we constructed 5 MCU truncation mutants, each with a C-terminal FLAG tag (Fig. 1B): mutants lacking His51-Leu100 (Δ51–100), Lys101-Leu150 (Δ101–150), Val151-Cys190 (Δ151–190), Ile191-Arg220 (Δ191–220), and Arg310-Glu350 (Δ310–350). When we introduced the expression vector of each MCU mutant together with that of EMRE into yeast, all truncation mutants were expressed at almost the same protein level as full-length MCU (Fig. 1C). Two immunoreactive bands were detected in each lane: the upper band contained immature MCU; and the lower one, mature MCU in which the MTS at the N-terminus had been processed (Fig. S1). In the case of each truncation mutant, the bands of mature MCU were clearly detected. As shown in Fig. 1D, the mitochondria isolated from yeast transformed by the empty vector were unable to take up Ca^{2+}; whereas the mitochondria from the transformant expressing full-length MCU and EMRE showed Ca^{2+} uptake activity. The mitochondria with Δ51–100 showed a slightly lower activity of calcium uptake than those with full-length MCU. On the other hand, the mitochondria with Δ101–150 and Δ151–190 showed about 50% lower Ca^{2+} uptake activities; and those with Δ191–220 and Δ310–350 had completely lost the activity, thus indicating that Ile191-Arg220 and Arg310-Glu350 were critical regions for MCU function. To understand the reasons why Δ191–220 and Δ310–350 lacked the Ca^{2+} uptake activity, we confirmed the intracellular localization of these 2 loss-of-function mutants by using mutants with EGFP fused to their C-terminus. Both truncation mutants were localized in mitochondria like the full-length MCU, indicating that the loss of function of these mutants was at least not due to any disorder of their translocation to the mitochondria (Fig. 1E).

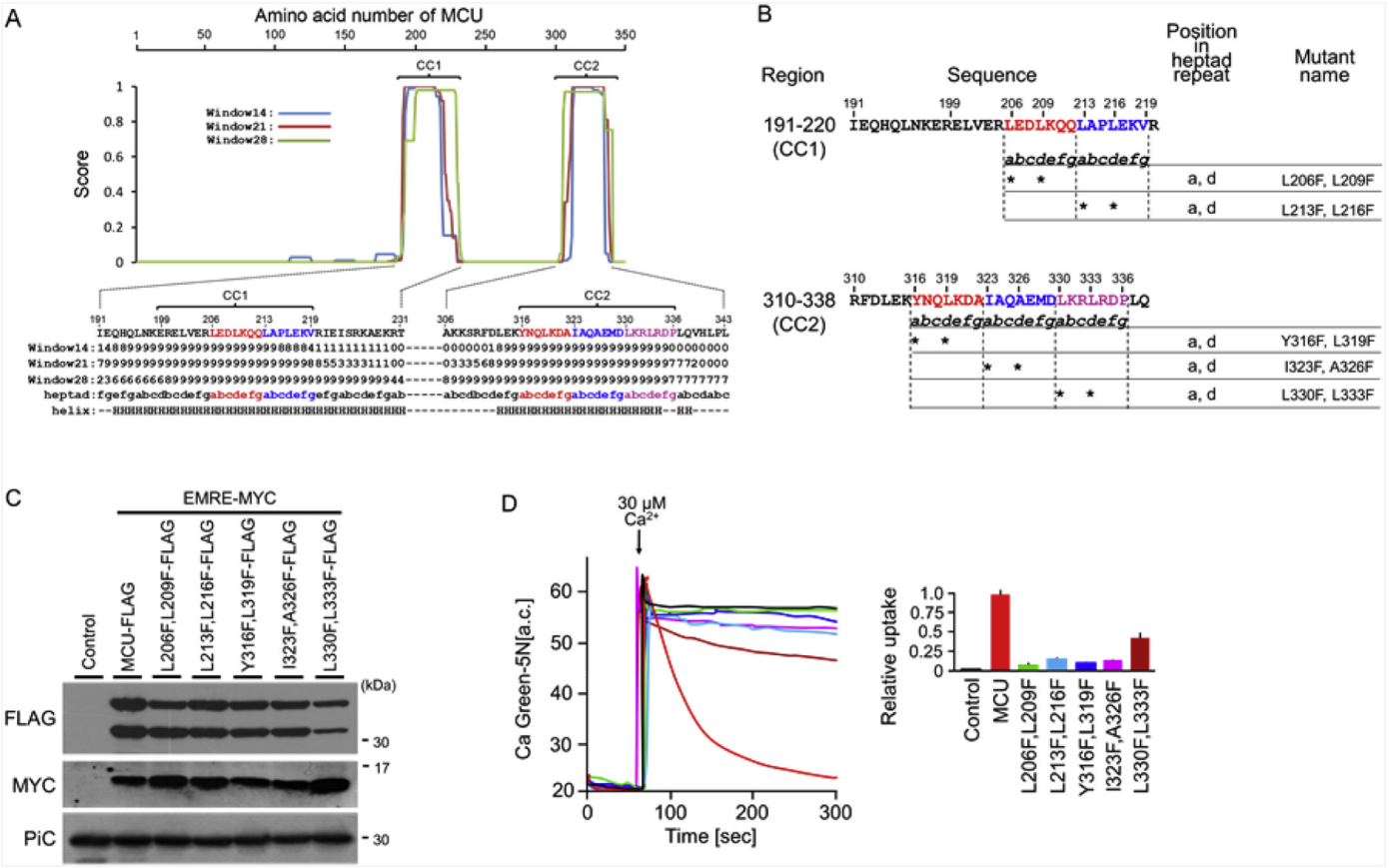

Fig. 2. Effects of coiled-coil domains of MCU on the mitochondrial Ca^{2+} uptake. (A), Predicted coiled-coil motifs. A Probability plot for the coiled-coil motifs in mouse MCU as predicted by COILS server using the MTDIK scoring matrix. Probability scores on a scale of 0–1 (1 is 100%) on the vertical axis are plotted against the aa residue number on the horizontal axis. Peaks in the graph indicate regions of higher coiled-coil probability. The default output of probabilities in the scanning windows of 14, 21, and 28 aa residues are shown in blue, red, and green, respectively. The predicted coiled-coil motifs are labeled as CC1 and CC2, respectively. The probability scores (a score of 9 is equivalent to 100% probability) in the scanning windows of 14, 21, and 28, in the region are shown below the respective amino-acid sequence. The heptad frame (*abcdefg*) for scoring the probabilities and the secondary structure as predicted by MLRC are shown below the probability scores. (B), Asterisks indicate the mutated amino acids that corresponded to the *a* and *d* positions in each predicted 7-amino-acid heptad coil. (C), Immunoblots of mitochondria isolated from yeast expressing the above-indicated FLAG-tagged MCU 2-point mutants together with MYC-tagged EMRE. The mitochondrial phosphate carrier (PiC) was used as a loading control for mitochondria. (D), Mitochondrial Ca^{2+} uptake; Left: representative traces of calcium uptake by mitochondria from the transformants having the indicated proteins, with 30 μM $CaCl_2$ added at the time indicated by the arrow. Right: Relative rates of Ca^{2+} uptake defined as the change in luminescence at 150 s, normalized by the uptake in the mitochondria bearing MCU-FLAG and EMRE-MYC (mean ± s.d.); n ≥ 3.

3.2. Functional analysis of the 2 coiled-coil domains in mouse MCU

Ile191-Arg220 and Arg310-Glu350 of mouse MCU were predicted to contain the coiled-coil domains, which are conserved in the MCUs of various species [27]. To analyze these domains in detail, we subjected the protein sequence of mouse MCU to the statistical analysis program of the COILS server [42] (Fig. 2A). This server analysis suggested the presence of 2 regions containing a coiled-coil domain. In the coiled-coil probability plot using the scanning window of 14, 21, and 28 aa residues, high scores were commonly detected in Glu199-Val219 and Tyr316-Pro336, which were contained in CC1 (Ile191-Arg220) and CC2 (Arg310-Gln338), respectively. Coiled-coil domains consist of typical heptad repeats with residues labeled as *abcdefg* [42,43]. At least, 5 heptads, $LEDLKQQ_{206–212}$, $LAPLEKV_{213–219}$, $YNQLKDA_{316–322}$, $IAQAEMD_{323–329}$, and $LKRLRDP_{330–336}$, were predicted in all 3 scanning windows (Fig. 2B). Each heptad repeat of the coiled-coil domain has specific hydrophobic residues at the *a* and *d* positions (noted by asterisks in Fig. 2B), which residues are critical for the coiled-coil interactions [42,43]. To examine whether the formation of this coiled coil in CC1 and/or CC2 was essential for Ca^{2+} uptake activity, we constructed two-point mutants, in which both amino acid residues at the *a* and *d* positions in the predicted coiled-coil domains of MCU were substituted to phenylalanine residues: $CC1_{L206F,L209F}$, $CC1_{L213F,L216F}$, $CC2_{Y316F,L319F}$, $CC2_{I323F,A326F}$, $CC2_{L330F,L333F}$ (Fig. 2B). It was expected that phenylalanine residues at these positions would retain the hydrophobicity of the helix itself, but would disrupt helix-helix interactions due to the "bulkiness" of the phenylalanine [43–45]. All 2-point mutants were expressed at almost the same protein level as native MCU (Fig. 2C). Although the mitochondria with $CC2_{L330F,L333F}$ showed weak Ca^{2+} uptake activity, the mitochondria with other mutants showed almost no Ca^{2+} uptake activities (Fig. 2D), thus indicating that the formation of the coiled coil in CC1 and CC2 of MCU was also critical for Ca^{2+} uptake activity. However, the partner molecule of CC1 or CC2 for each coiled coil could not be known from only this result.

3.3. Functional analysis of CC1 and CC2 of MCU in yeast mitochondria lacking FMP32

Tomar et al. reported that the CC1 in MCU interacts with a coiled-coil region in MCUR1 in the mitochondria of COS7 cells [24]. FMP32 is a MCUR1 homolog in yeast [46]. Prediction by the COILS server showed that FMP32 also contains a conserved coiled-coil region in its Ala100-Gly136 (Fig. S2). Thus, also in our experimental system, the functional importance of the coiled-coil domains of mouse MCU in Ca^{2+} uptake function is possibly related to FMP32. To verify this possibility, we first examined whether FMP32 would affect the calcium

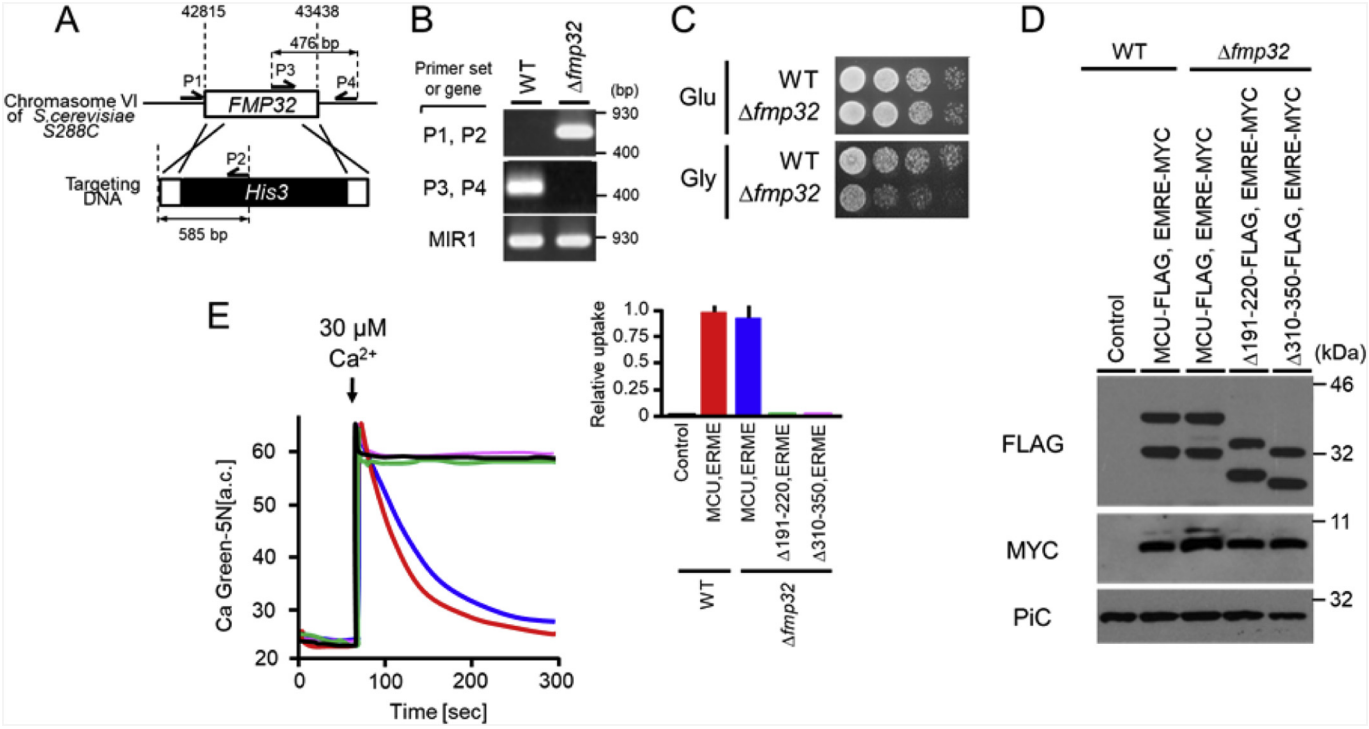

Fig. 3. Effects of FMP32 on the critical role of coiled-coil domains in Ca^{2+} uptake. (A), Deletion of the *FMP32* gene of *S. cerevisiae* by homologous recombination. The *FMP32* gene is encoded in nucleotides 42,815–43,438 of chromosome VI of *S. cerevisiae S288C*. *HIS3* gene and its flanking sequences are encoded in nucleotides 169–1375 of yeast centromere vector pRS313. Targeting DNA coded for the *HIS3* gene fused to nucleotides 42,815–42,874 of chromosome VI at its 5′ terminus and 43,379–43,438 at its 3′ terminus. P1-P4 indicate the positions of primers used in the PCR to confirm deletion of the *FMP32* gene; and the sequences of the primers are described in Table S1. (B), PCR amplification for genotyping of Δ*fmp32*. Genomic DNAs isolated from WT yeast and Δ*fmp32* were subjected to PCR using the indicated primer sets or primer set for MIR1 (mitochondrial phosphate carrier: NM_001181735.1). (C), Growth-defect phenotype of wild-type yeast cells (WT) and yeast cells lacking the *FMP32* gene (Δ*fmp*32) on YP plates including 2% glucose or 3% glycerol. After incubation at 37 °C for 3 days, cell growth on the plates was assessed photographically. (D), Immunoblots of mitochondria isolated from yeast expressing the above-indicated FLAG-tagged MCU deletion mutants together with MYC-tagged EMRE. The mitochondrial phosphate carrier (PiC) was used as a loading control for mitochondria. (E), Mitochondrial Ca^{2+} uptake. Left: representative traces of calcium uptake by mitochondria from the transformants having the indicated proteins, with 30 μM $CaCl_2$ added at the time indicated by the arrow. Right: Relative rates of Ca^{2+} uptake defined as the change in luminescence at 150 s, normalized by the uptake in the mitochondria of WT yeast expressing MCU-FLAG and EMRE-MYC (mean ± s.d.); n ≥ 3.

uptake function of yeast mitochondria expressing MCU and EMRE. For this, we prepared a Δ*fmp32* strain by homologous recombination (Fig. 3A). When the genomic DNA from this Δ*fmp32* strain was subjected to PCR using 2 primer sets (P1-P2 and P3-P4), the deletion of FMP32 from the genomic DNA was confirmed (Fig. 3B). The Δ*fmp32* strain showed normal growth in glucose-supplemented media; however, when it was grown on a non-fermentable carbon source (glycerol), a growth defect was observed at 37 °C (Fig. 3C). This phenotype of the Δfmp32 strain agreed with that previously reported [46]. Next, the Δ*fmp32* strain was transformed by using the expression vector for full-length MCU, Δ191–220 or Δ310–350 together with that for EMRE; and from the obtained transformants, the mitochondria were isolated. The protein levels of full-length MCU or MCU mutants in the transformants of the Δ*fmp32* strain were almost the same as those in the wild-type yeast (Fig. 3D). Furthermore, the mitochondria from the Δ*fmp32* strain expressing MCU and EMRE showed almost the same Ca^{2+} uptake activity as those from the wild-type strain expressing MCU and EMRE; however, the mitochondria from the Δ*fmp32* strain expressing Δ191–220 or Δ310–350 with EMRE had lost their Ca^{2+} uptake activity (Fig. 3E). These results were the same as those for the mitochondria from the wild-type strain expressing Δ191–220 or Δ310–350 (Fig. 1D). These results showed that, at least in yeast mitochondria, FMP32 did not affect the functions of MCU reconstituted in the mitochondria, indicating that the functional importance of the coiled-coil domains of MCU in the calcium uptake was unrelated to the function of FMP32.

3.4. Importance of the 2 coiled-coil domains of D. discoideum MCU in Ca^{2+} uptake function

From mammals to some fungi, the EMRE is a critical factor for mitochondrial Ca^{2+} uptake function [18]. Furthermore, the interaction of EMRE with MCU is essential for the Ca^{2+} uptake, but the reasons why this interaction is needed has been unclear [26,47]. Thus, it is interesting to determine whether the functional importance of the 2 coiled-coil domains of MCU would be related to EMRE. In the mouse, MCU and EMRE are essential for the calcium uptake function; but, in a certain fungus, *D. discoideum* (Dd), a MCU homolog (DdMCU) is encoded in the genome but Dd has no homolog of the EMRE [18] (Fig. 4A). Actually, DdMCU expressed in yeast enables Ca^{2+} uptake by the mitochondria even in the absence of EMRE [25]. To investigate the relationships between the coiled-coil domains of MCU and EMRE, we next reconstituted DdMCU in yeast mitochondria; and using the mitochondria, we examined the functional roles of the coiled-coil domains in EMRE-independent mitochondrial Ca^{2+} uptake by DdMCU. The DdMCU has a shorter N-terminal region than that of the mouse MCU, but the C-half region of DdMCU (Val125-Lys275) exhibits strong sequence homology to that of mouse MCU (Fig. S3). DdMCU shares domain organization with mouse MCU: N-terminal MTS, 2 coiled-coil domains surrounding 2 transmembrane domains that flank the WDxxEP motif (Fig. 4B). Indeed, when DdMCU having a FLAG tag fused at its C-terminus was expressed alone in yeast (see the lane noted by "Dd MCU-FLAG" in Fig. 4C), the DdMCU by itself enabled yeast mitochondria to take up Ca^{2+} even in the absence of EMRE (see the trace and histogram

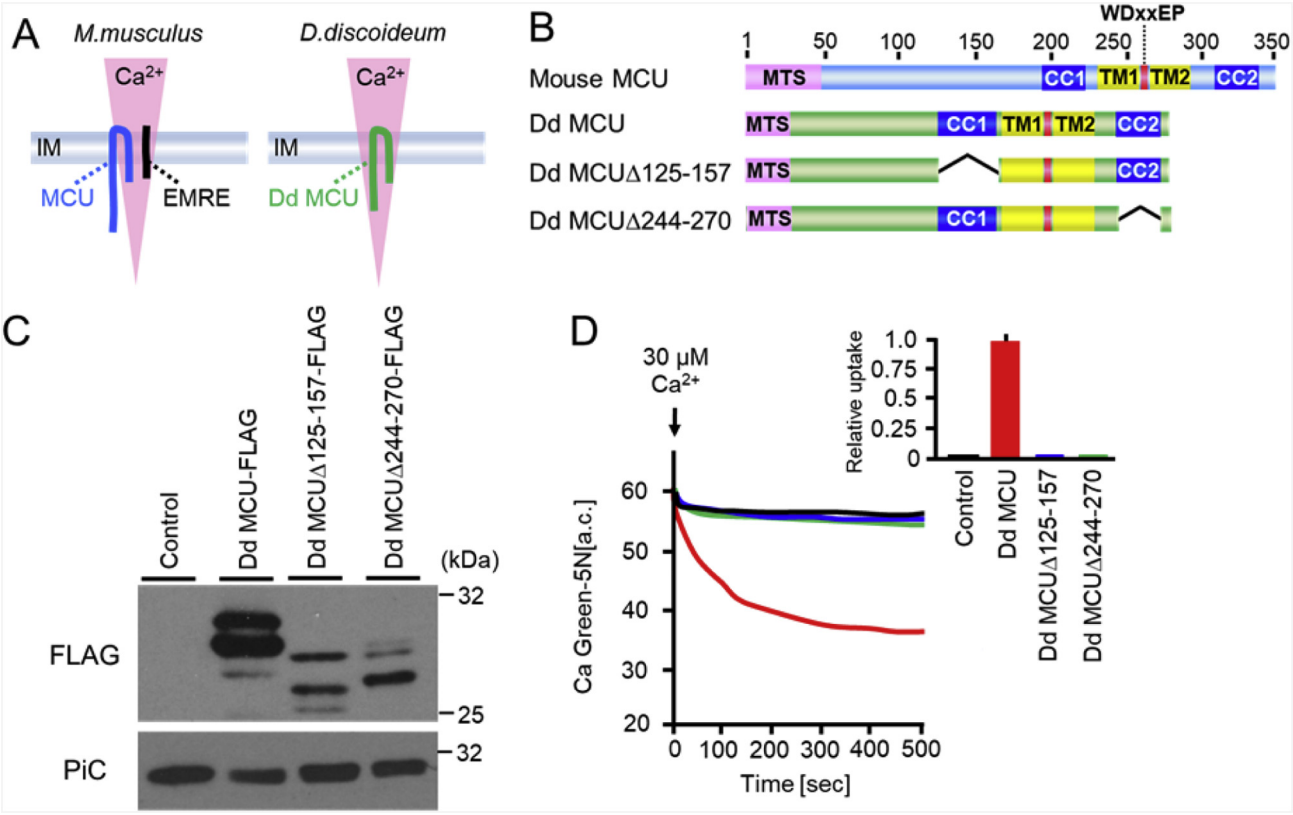

Fig. 4. Roles of coiled-coil domains of *D. discoideum* MCU in Ca^{2+} uptake activity. (A), In the mouse (*M. musculus*), MCU and EMRE are essential for mitochondrial Ca^{2+} uptake; in fungi (*D. discoideum*), MCU (DdMCU) alone is essential. IM, mitochondrial inner membrane. (B), Schematic representation of full-length DdMCU and its deletion mutants, showing predicted domains and motif: the mitochondrial translocation signal (MTS) at Met1-Leu28; coiled-coil regions (CC1 and CC2) at Val125-Arg157 and Pro244-Lys270, respectively; transmembrane regions (TM1 and TM2) at Ile166-Trp186 and Ile193-Phe213, respectively; and WDxxEP motif at Trp191-Pro196. (C), Immunoblots of mitochondria isolated from yeast expressing the above-indicated FLAG-tagged DdMCU deletion mutants. The mitochondrial phosphate carrier (PiC) was used as a loading control for mitochondria. (D), Mitochondrial Ca^{2+} uptake. Left: representative traces of calcium uptake by mitochondria from the transformants having the indicated proteins, with 30 μM $CaCl_2$ added at the time indicated by the arrow. Right: Relative rates of Ca^{2+} uptake defined as the change in luminescence at 300 s, normalized by the uptake in the mitochondria of WT yeast expressing DdMCU-FLAG (mean ± s.d.); n ≥ 3.

in red in Fig. 4D), a result agreeing with the previous report by Kovacs-Bogdan et al. [25]. Next, we investigated the functional roles of the coiled-coil domains of DdMCU in mitochondrial Ca^{2+} uptake. We constructed 2 DdMCU mutants lacking Val125-Arg157 or Pro244-Lys270, which were predicted as coiled-coil domains of DdMCU, each with a C-terminal FLAG tag: DdMCUΔ125-157 and DdMCUΔ244-270 (Fig. 4B). Then we transformed the yeast with the expression vector of each DdMCU mutant. Both DdMCU mutant proteins were detected in the mitochondria from each transformant (Fig. 4C). As a result of monitoring of the Ca^{2+} uptake activity, the mitochondria with neither DdMCUΔ125-157 nor DdMCUΔ244-270 showed the Ca^{2+} uptake activity (Fig. 4D); this result corresponded to that found for the mouse MCU mutants lacking either coiled-coil domain (Fig. 1). This finding suggested that the critical roles of coiled-coil domains of MCU in Ca^{2+} uptake function were independent of the EMRE.

4. Discussion

MCU is conserved among various species. In all MCUs, 2 coiled-coil domains (CC1 and CC2) as well as the WDxxEP motif are conserved in them. Although the functional roles of the WDxxEP motif of MCU in mitochondrial Ca^{2+} uptake have been well examined [12,13], the functional roles of the coiled-coil domains have not yet been investigated. In this study, we revealed that both CC1 and CC2 in the mouse MCU play a critical role in mitochondrial Ca^{2+} uptake function (Fig. 1); and the analyses using point mutants suggested that the formation of the coiled-coil structure of CC1 and CC2 was critical (Fig. 2). Furthermore, the functional importance of CC1 and CC2 was independent of a yeast MCUR1 homolog (FMP32) and EMRE; MCUR1 and EMRE are considered as a regulator and as an activator of the MCU-forming pore, respectively (Figs. 3, 4), indicating that CC1 and CC2 of MCU play a critical role in the pore-forming function of MCUs themselves, at least in yeast. On the other hand, MCUs also have a conserved N-terminal domain (NTD), which is located in the Val74-Arg164 sequence in mouse MCU. We showed that deletion of the amino acid region including the NTD (His51-Leu100, Lys101-Leu150, Val151-Cys190) caused lower Ca^{2+} uptake activity, indicating that NTD was also related to the regulation of Ca^{2+} uptake function (Fig. 1). Lee et al. revealed the X-ray structure of the NTD, and the structure and additional findings made by using mammalian cell lines led them to conclude that a phosphorylation-induced conformational change in NTD regulates the Ca^{2+} uptake function [29]. To reveal the details of this regulatory mechanism involving the NTD, more study will be needed.

Mammals possess 2 apparent yeast FMP32 homologs, i.e. CCDC90A (MCUR1) and CCDC90B. The amino acid sequence of FMP32 is more similar to that of CCDC90B than to that of MCUR1, suggesting that CCDC90B but not MCUR1 might be the genuine FMP32 homolog. Importantly, CCDC90B has been shown to physically interact with MCU, but not affected on mitochondrial Ca^{2+} uptake [24]. Therefore, the experiments we here performed using FMP32 null yeasts do not completely rule out the possibility that coiled-coil domains in MCU functionally required MCUR1.

Using NMR Oxianoid et al. examined the structure of N-terminal domain-deleted worm MCU and found that this MCU formed a

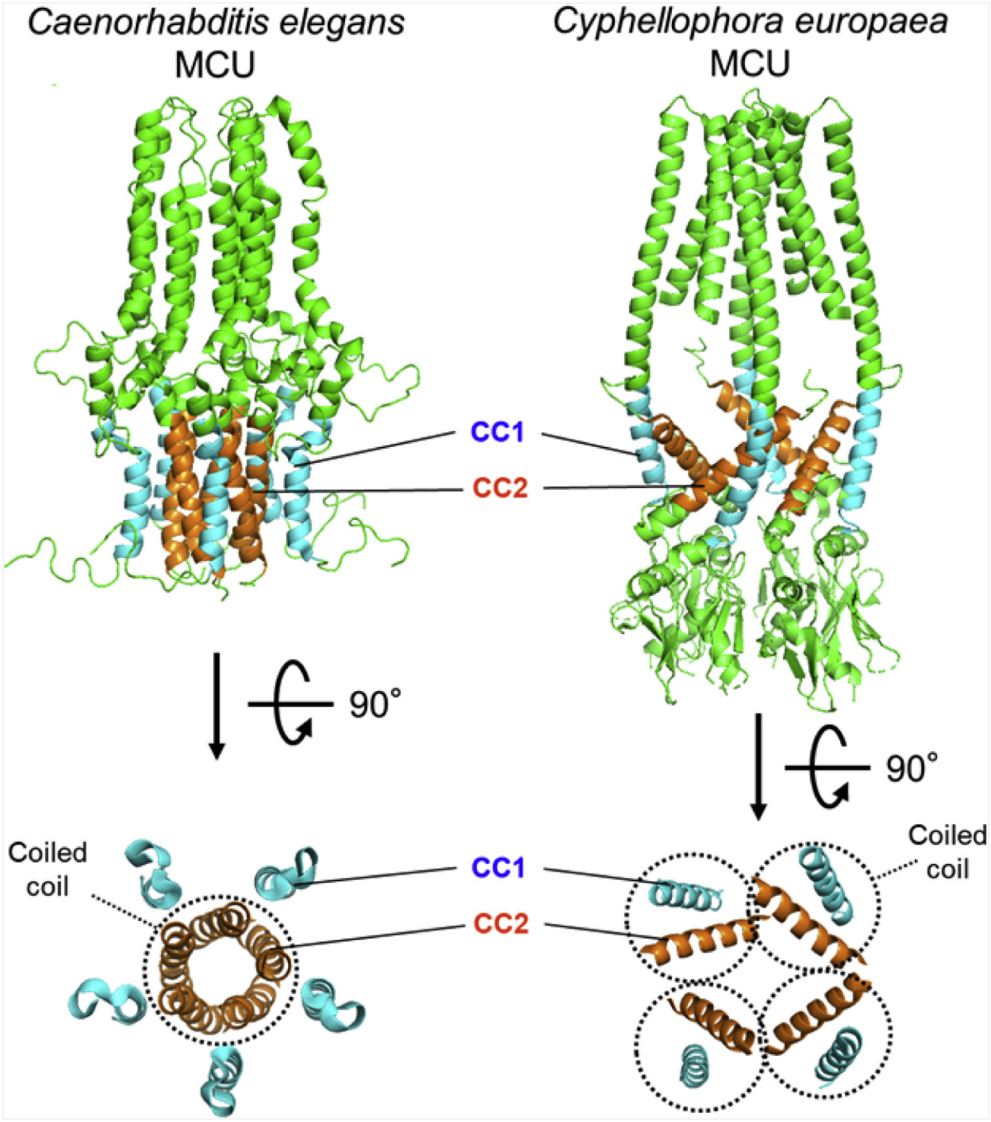

Fig. 5. Comparison between the coiled-coil structures of the NMR-determined structure of NTD-lacking *Caenorhabditis elegans* MCU and the cryo-EM structure of *Cyphellophora europaea* MCU. **Left**, the structure of NTD-lacking *C. elegans* MCU (PDB ID: 5ID3); **Right**, the structure of *C. europaea* MCU (PDB ID: 6DNF). CC1 and CC2 are shown in blue and orange, respectively: in *C. elegans* MCU (Uniprot ID: Q21121), CC1 and CC2 were located in Lys180-Leu193 and Gln289-Pro316, respectively; and in *C. europaea* MCU (Uniprot ID: W2SDE2), in Leu166-Ala182 and Leu278-Arg292, respectively [30,34].

pentamer [30]. In the pentameric structure, 5 CC2s formed a pentameric coiled coil; on the other hand, the CC1s did not form any coiled-coil structure, though they formed an α-helix (Fig. 5, left). Recently, by use of cryo-EM and X-ray analysis 4 independent groups showed full-length fungal MCUs to have a tetrameric structure [31–34]. The reason for the structural discrepancy between the tetramers of fungal MCUs and the pentamer of worm MCU remains unclear. In the tetramer models, the coiled coil was formed by CC1 and CC2 positioned in an antiparallel manner. A central space surrounded by the 4 coiled coils was created; and CC1 and CC2 were located outside and inside of the central space, respectively (Fig. 5, right). However, in the recent studies on the structures of fungal MCUs, the connection between TM2 and CC2 has remained uncertain. Thus, it is unclear whether the coiled coil formed by CC1 and CC2 is an inter-protomer structure or an intra-protomer structure. The biochemical findings that we here acquired corresponded to the tetramer model: our experiment showed the non-functionality of MCU mutations with point mutations in the CC1, which does not participate in the coiled-coil in the pentamer model but does participate in that in the tetramer one (Figs. 2D and 5). The formation of the coiled coil in CC1 and CC2 was critical for the mitochondrial Ca^{2+} uptake. Our results suggest that, at least in the open state, MCUs formed tetramers, but not pentamers, on the mitochondrial inner membrane.

Baradaran et al. reported the cryo-EM reconstruction of *Cyphellophora europaea* MCU (ceMCU) tetramers at a 3.2 Å resolution [34]. Additionally, they also examined the cryo-EM structure of zebrafish MCU by cryo-EM reconstruction at 8.5 Å resolution. As a result, although all α-helices of zebra finch MCU were unable to be resolved in the cryo-EM density map, the overall structure of zebrafish MCU was similar to that of the ceMCU. Since the mouse MCU has 77% identity and 95% similarity to the zebrafish MCU, the structure of mouse MCU is considered to be highly similar to that of the zebrafish MCU. We here predicted our mouse MCU homology model by using SWISS MODEL based on the cryo-EM structure of ceMCU tetramer, which was resolved at high resolution [48]. In this model, CC1 and CC2 formed a coiled coil in an antiparallel manner (Fig. 6); and this manner and the structure of coiled coil were just like those of the CC1 and CC2 of ceMCU and *Neurospora crassa* MCU, which were analyzed by cryo-EM (Figs. S4 and S5). In the coiled coil of the mouse MCU model, Leu206, Leu209, and Leu213, which were located in CC1, and Leu319, Ile323, and Ala326,

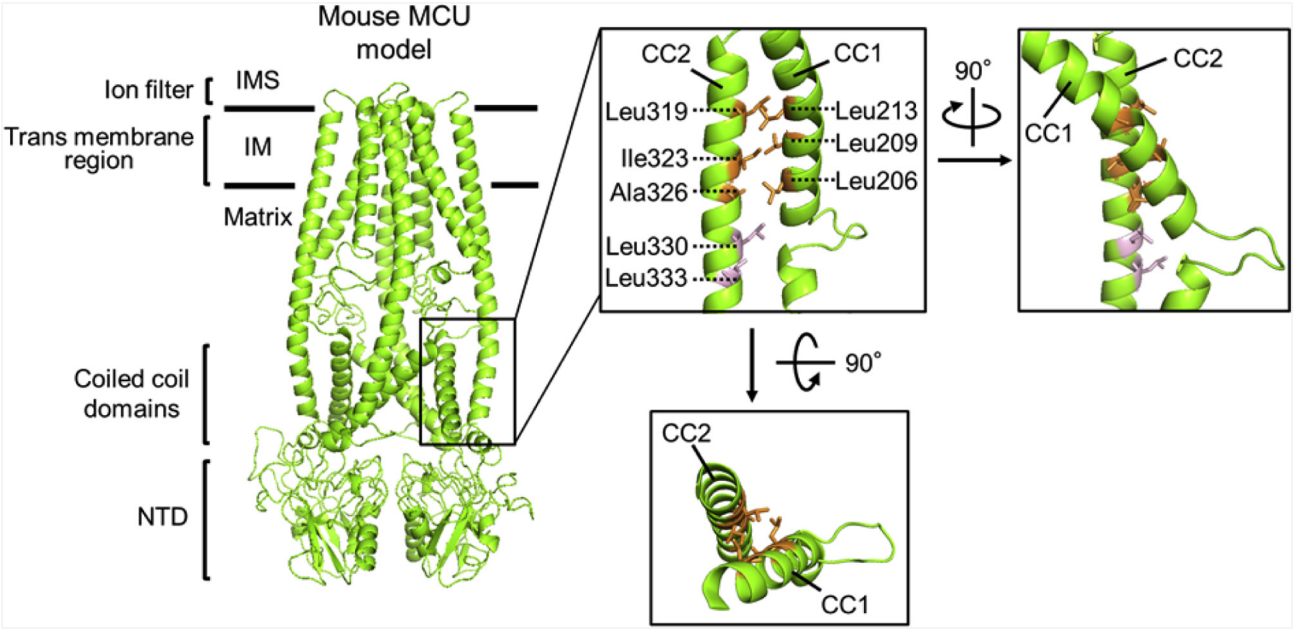

Fig. 6. Coiled-coil structure in the mouse MCU model. **Left**, whole view of mouse MCU model based on the structure of *C. europaea* MCU determined by using SWISS MODEL. **Middle** and **Right**, Close-up views of the coiled-coil structure. The hydrophobic amino-acid residues located at the position where CC1 and CC2 were the closest to one another are shown in orange; and Leu330 and Leu333, in pink.

located in CC2, are hydrophobic amino acid residues located at the position where CC1 and CC2 came closest to each other; and probably, at that position, CC1 and CC2 would be in contact with each other (see the close-up views of Fig. 6). These hydrophobic amino acid residues located at the predicted contact site of CC1 and CC2 (Leu206, Leu209, Leu213, Leu319, Ile323, Ala326) were consistent with the amino acid residues which we here muted to prepare the loss-of-function MCU mutants (Fig. 2; $CC1_{L206F,L209F}$, $CC1_{L213F,L216F}$, $CC2_{Y316F,L319F}$, $CC2_{I323F,A326F}$). On the other hand, as was shown in Fig. 2E, the mitochondria with $CC2_{L330F,L333F}$ did not completely lose Ca^{2+} uptake activity but showed weak activity; and this result also was consistent with the previous finding about the structural location of Leu330 and Leu333, which were a little apart from the predicted contact site of CC1 and CC2 (see the amino acid residues colored in pink in the close-up views of Fig. 6).

Why is the coiled-coil structure formed by CC1 and CC2 critical for the Ca^{2+} uptake function? In the fungal MCU tetramer models and the homology model of mouse MCU, there is, below the transmembrane regions, ample space possible for Ca^{2+} to diffuse between the transmembrane region and the coiled-coil domain (Fig. 7, left) [31–34]. Thus, the MCU tetramer has not only the filter structure, located in the inter membrane space side, selectively to import Ca^{2+} into the inside of the MCU tetramer, but also the opening structure, located in the middle of the tetramer, to diffuse the Ca^{2+} from the inside of the MCU tetramer into the matrix (Fig. 7, middle). Those MCU tetramer models led us to the following hypothesis: the coiled coils by CC1 and CC2 are formed so as to create the Ca^{2+}-diffusion space in the way that CC2 pushes up CC1 (see the blue and orange helixes in Fig. 7) as if an umbrella is opened by the support of its ribs (Fig. 7, middle). Thus, the reason why the point mutations, which were expected to inhibit the formation of the coiled coil by CC1 and CC2, decreased the Ca^{2+} uptake activity (Fig. 2) might be that the space for Ca^{2+} diffusion became narrower because of the deformation of the coiled coil, as if the umbrella had lost the support of its ribs and closed (Fig. 7, right). Therefore, the coiled coil formed by CC1 and CC2 may play a role to fix the channel pore in the open state, like a stopper ring with which the ribs can keep the umbrella open. To confirm whether or not this model is correct, structural analysis and computer simulation analysis of MCU mutants that are unable to form the coiled-coil structure will be needed.

Most coiled coils observed in proteins have > 10 repeats of heptad length [49]. However, the length of the coiled coil of MCU was comparatively short; CC1 and CC2 had about 3 repeats of heptad length of coiled coil consisting of about 20 amino acid residues. The mechanosensitive channel of large conductance (MscL) of *Mycobacterium tuberculosis* is also a membrane protein with a short-length coiled coil. MscL having 2 transmembrane regions forms a pentamer in the plasma membrane of the bacteria. MscL has a short α helical region consisting of 18 amino acid residues in its carboxyl terminal domain, which region forms a pentameric coiled coil in the cytoplasm in the closed state [50,51]; and on full opening, the cytoplasmic helices are suggested to become disassembled and to move onto the surface of the plasma membrane [52]. Since the coiled coil length of CC1 and CC2 of MCU are also short, the coiled coils might not interact strongly with each other; thus, even if the coiled coil becomes unstable due to some stimuli, it would be possible that the Ca^{2+} uptake activity of MCU could be regulated by the stability of the coiled coil. The coiled-coil domains of MCU might function as a switch to regulate mitochondrial Ca^{2+} uptake.

Very recently, Wang et al. reported the structure of the human MCU-EMRE complex based on cryo-EM at 3.6 Å resolution [53]. In this model, the human MCU tetramer formed a channel with 1 EMRE bound to each MCU. Regarding the coiled-coil domains of MCU, their model showed the following: 1) CC1 and CC2b (corresponding to CC2 in mouse MCU) formed the coiled coil; 2) EMRE bound to the transmembrane domain (TM1) of MCU but not to the coiled-coil domains; 3) in the coiled coil of the human MCU, Leu207, L210, and L214 (corresponding to Leu206, Leu209, and Leu213 in mouse MCU, respectively) which were located in CC1, and Ile320, Ile324, and Ala327 (corresponding to Leu319, Ile323, and Ala326 in mouse MCU, respectively), located in CC2b, are hydrophobic amino acid residues located at the position where CC1 and CC2b came closest to each other; and, probably, that position would be the contact site of CC1 and CC2b (Fig. S6). This information regarding the coiled-coil structure in the human MCU model also corresponded to the biochemical findings that we have reported herein.

In the present study, we showed that the formation of the coiled coils in CC1 and CC2 of mouse MCU was of functional importance, one

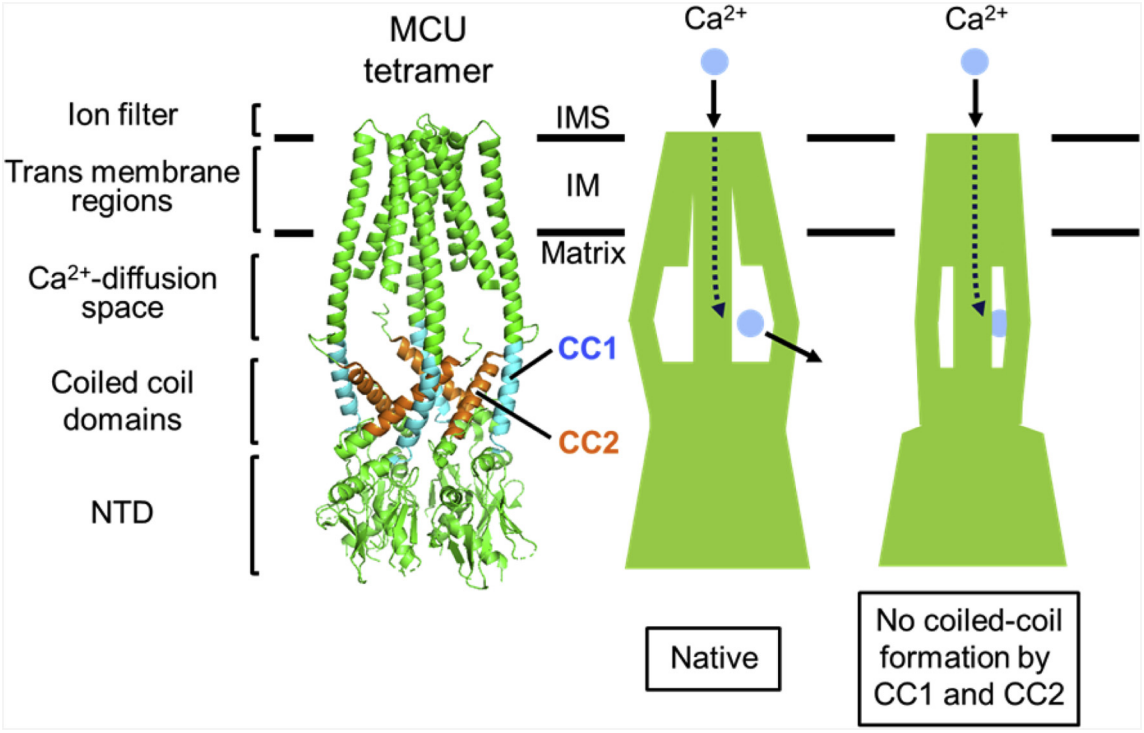

Fig. 7. Functional model of coiled-coil domains of MCU. **Left**, structure of *C. europaea* MCU. **Middle**, there is ample space possible for Ca^{2+} to diffuse between the transmembrane region and coiled-coil domain; thus, Ca^{2+} which has passed the Ca^{2+}-selective filter is considered to mainly enter into matrix through this space. **Right**, when the formation of the coiled coil is inhibited by deletion or point mutation, the space for Ca^{2+} diffusion would become narrow, as in the case of an umbrella that is closed, resulting in a probable decrease in Ca^{2+} uptake activity.

that was independent of the regulatory subunits of the calcium uniporter complex other than MCU. Our findings indicated the tetrameric structure of the MCU, not the pentameric one, providing a clue to the support of MCU functions in the mitochondrial membrane. Moreover, our data also have provided new insight into the molecular mechanisms underlying the uptake of Ca^{2+} by the MCU.

Supplementary data to this article can be found online at https://doi.org/10.1016/j.bbabio.2019.148061.

Transparency document

The Transparency document associated with this article can be found, in online version.

Acknowledgements

This work was supported by JSPS KAKENHI (Grant Numbers JP17K08275 and JP17K08274) and by Takeda Science Foundation. The authors thank Dr. Yoshiaki Yano (Graduate School of Pharmaceutical Sciences, Kyoto University) for useful discussions.

References[1]

[1] J.G. McCormack, R.M. Denton, The role of mitochondrial Ca^{2+} transport and matrix Ca^{2+} in signal transduction in mammalian tissues, Biochim. Biophys. Acta 1018 (1990) 287–291.
[2] P. Pizzo, I. Drago, R. Filadi, T. Pozzan, Mitochondrial Ca^{2+} homeostasis: mechanism, role, and tissue specificities, Pflugers Arch. 464 (2012) 3–17.
[3] D. Pendin, E. Greotti, T. Pozzan, The elusive importance of being a mitochondrial Ca^{2+} uniporter, Cell Calcium 55 (2014) 139–145.
[4] P. Bernardi, Mitochondrial transport of cations: channels, exchangers, and permeability transition, Physiol. Rev. 79 (1999) 1127–1155.
[5] V. Giorgio, S. von Stockum, M. Antoniel, A. Fabbro, F. Fogolari, M. Forte, G.D. Glick, V. Petronilli, M. Zoratti, I. Szabo, G. Lippe, P. Bernardi, Dimers of mitochondrial ATP synthase form the permeability transition pore, Proc. Natl. Acad. Sci. U. S. A. 110 (2013) 5887–5892.
[6] V. Giorgio, V. Burchell, M. Schiavone, C. Bassot, G. Minervini, V. Petronilli, F. Argenton, M. Forte, S. Tosatto, G. Lippe, P. Bernardi, Ca^{2+} binding to F-ATP synthase β subunit triggers the mitochondrial permeability transition, EMBO Rep. 18 (2017) 1065–1076.
[7] C.P. Baines, R.A. Kaiser, N.H. Purcell, N.S. Blair, H. Osinska, M.A. Hambleton, E.W. Brunskill, M.R. Sayen, R.A. Gottlieb, G.W. Dorn, J. Robbins, J.D. Molkentin, Loss of cyclophilin D reveals a critical role for mitochondrial permeability transition in cell death, Nature 434 (2005) 658–662.
[8] E. Palma, T. Tiepolo, A. Angelin, P. Sabatelli, N.M. Maraldi, E. Basso, M.A. Forte, P. Bernardi, P. Bonaldo, Genetic ablation of cyclophilin D rescues mitochondrial defects and prevents muscle apoptosis in collagen VI myopathic mice, Hum. Mol. Genet. 18 (2009) 2024–2031.
[9] T.E. Gunter, D.R. Pfeiffer, Mechanisms by which mitochondria transport calcium, Am. J. Phys. 258 (1990) C755–C786.
[10] Y. Kirichok, G. Krapivinsky, D.E. Clapham, The mitochondrial calcium uniporter is a highly selective ion channel, Nature 427 (2004) 360–364.
[11] J. Santo-Domingo, N. Demaurex, Calcium uptake mechanisms of mitochondria, Biochim. Biophys. Acta 1797 (2010) 907–912.
[12] D. De Stefani, A. Raffaello, E. Teardo, I. Szabo, R. Rizzuto, A forty-kilodalton protein of the inner membrane is the mitochondrial calcium uniporter, Nature 476 (2011) 336–340.
[13] J.M. Baughman, F. Perocchi, H.S. Girgis, M. Plovanich, C.A. Belcher-Timme, Y. Sancak, X.R. Bao, L. Strittmatter, O. Goldberger, R.L. Bogorad, V. Koteliansky, V.K. Mootha, Integrative genomics identifies MCU as an essential component of the mitochondrial calcium uniporter, Nature 476 (2011) 341–345.
[14] F. Perocchi, V.M. Gohil, H.S. Girgis, X.R. Bao, J.E. McCombs, A.E. Palmer, V.K. Mootha, MICU1 encodes a mitochondrial EF hand protein required for Ca^{2+} uptake, Nature 467 (2010) 291–296.
[15] M. Plovanich, R.L. Bogorad, Y. Sancak, K.J. Kamer, L. Strittmatter, A.A. Li, H.S. Girgis, S. Kuchimanchi, J. De Groot, L. Speciner, N. Taneja, J. Oshea, V. Koteliansky, V.K. Mootha, MICU2, a paralog of MICU1, resides within the mitochondrial uniporter complex to regulate calcium handling, PLoS One 8 (2013) e55785.
[16] K. Mallilankaraman, C. Cardenas, P.J. Doonan, H.C. Chandramoorthy, K.M. Irrinki, T. Golenar, G. Csordas, P. Madireddi, J. Yang, M. Muller, R. Miller, J.E. Kolesar, J. Molgo, B. Kaufman, G. Hajnoczky, J.K. Foskett, M. Madesh, MCUR1 is an essential component of mitochondrial Ca^{2+} uptake that regulates cellular metabolism, Nat. Cell Biol. 14 (2012) 1336–1343.
[17] A. Raffaello, D. De Stefani, D. Sabbadin, E. Teardo, G. Merli, A. Picard, V. Checchetto, S. Moro, I. Szabo, R. Rizzuto, The mitochondrial calcium uniporter is a multimer that can include a dominant-negative pore-forming subunit, EMBO J. 32 (2013) 2362–2376.

[1] [Not checked so as to reduce correction time and thus cost]

[18] Y. Sancak, A.L. Markhard, T. Kitami, E. Kovacs-Bogdan, K.J. Kamer, N.D. Udeshi, S.A. Carr, D. Chaudhuri, D.E. Clapham, A.A. Li, S.E. Calvo, O. Goldberger, V.K. Mootha, EMRE is an essential component of the mitochondrial calcium uniporter complex, Science 342 (2013) 1379–1382.
[19] M. Patron, V. Checchetto, A. Raffaello, E. Teardo, D. Vecellio Reane, M. Mantoan, V. Granatiero, I. Szabo, D. De Stefani, R. Rizzuto, MICU1 and MICU2 finely tune the mitochondrial Ca^{2+} uniporter by exerting opposite effects on MCU activity, Mol. Cell 53 (2014) 726–737.
[20] M. Patron, V. Granatiero, J. Espino, R. Rizzuto, D. De Stefani, MICU3 is a tissue-specific enhancer of mitochondrial calcium uptake, Cell Death Differ. 26 (2019) 179–195.
[21] G. Pallafacchina, S. Zanin, R. Rizzuto, Recent advances in the molecular mechanism of mitochondrial calcium uptake, F1000Res 7 (2018).
[22] K.J. Kamer, Y. Sancak, Y. Fomina, J.D. Meisel, D. Chaudhuri, Z. Grabarek, V.K. Mootha, MICU1 imparts the mitochondrial uniporter with the ability to discriminate between Ca^{2+} and Mn^{2+}, Proc. Natl. Acad. Sci. U. S. A. 115 (2018) E7960–E7969.
[23] D. Chaudhuri, D.J. Artiga, S.A. Abiria, D.E. Clapham, Mitochondrial calcium uniporter regulator 1 (MCUR1) regulates the calcium threshold for the mitochondrial permeability transition, Proc. Natl. Acad. Sci. U. S. A. 113 (2016) E1872–E1880.
[24] D. Tomar, Z. Dong, S. Shanmughapriya, D.A. Koch, T. Thomas, N.E. Hoffman, S.A. Timbalia, S.J. Goldman, S.L. Breves, D.P. Corbally, N. Nemani, J.P. Fairweather, A.R. Cutri, X. Zhang, J. Song, F. Jana, J. Huang, C. Barrero, J.E. Rabinowitz, T.S. Luongo, S.M. Schumacher, M.E. Rockman, A. Dietrich, S. Merali, J. Caplan, P. Stathopulos, R.S. Ahima, J.Y. Cheung, S.R. Houser, W.J. Koch, V. Patel, V.M. Gohil, J.W. Elrod, S. Rajan, M. Madesh, MCUR1 is a scaffold factor for the MCU complex function and promotes mitochondrial bioenergetics, Cell Rep. 15 (2016) 1673–1685.
[25] E. Kovacs-Bogdan, Y. Sancak, K.J. Kamer, M. Plovanich, A. Jambhekar, R.J. Huber, M.A. Myre, M.D. Blower, V.K. Mootha, Reconstitution of the mitochondrial calcium uniporter in yeast, Proc. Natl. Acad. Sci. U. S. A. 111 (2014) 8985–8990.
[26] T. Yamamoto, R. Yamagoshi, K. Harada, M. Kawano, N. Minami, Y. Ido, K. Kuwahara, A. Fujita, M. Ozono, A. Watanabe, A. Yamada, H. Terada, Y. Shinohara, Analysis of the structure and function of EMRE in a yeast expression system, Biochim. Biophys. Acta 1857 (2016) 831–839.
[27] A.G. Bick, S.E. Calvo, V.K. Mootha, Evolutionary diversity of the mitochondrial calcium uniporter, Science 336 (2012) 886.
[28] J.D. Martell, T.J. Deerinck, Y. Sancak, T.L. Poulos, V.K. Mootha, G.E. Sosinsky, M.H. Ellisman, A.Y. Ting, Engineered ascorbate peroxidase as a genetically encoded reporter for electron microscopy, Nat. Biotechnol. 30 (2012) 1143–1148.
[29] Y. Lee, C.K. Min, T.G. Kim, H.K. Song, Y. Lim, D. Kim, K. Shin, M. Kang, J.Y. Kang, H.S. Youn, J.G. Lee, J.Y. An, K.R. Park, J.J. Lim, J.H. Kim, J.H. Kim, Z.Y. Park, Y.S. Kim, J. Wang, D.H. Kim, S.H. Eom, Structure and function of the N-terminal domain of the human mitochondrial calcium uniporter, EMBO Rep. 16 (2015) 1318–1333.
[30] K. Oxenoid, Y. Dong, C. Cao, T. Cui, Y. Sancak, A.L. Markhard, Z. Grabarek, L. Kong, Z. Liu, B. Ouyang, Y. Cong, V.K. Mootha, J.J. Chou, Architecture of the mitochondrial calcium uniporter, Nature 533 (2016) 269–273.
[31] J. Yoo, M. Wu, Y. Yin, M.A. Herzik Jr., G.C. Lander, S.Y. Lee, Cryo-EM structure of a mitochondrial calcium uniporter, Science 361 (2018) 506–511.
[32] N.X. Nguyen, J.P. Armache, C. Lee, Y. Yang, W. Zeng, V.K. Mootha, Y. Cheng, X.C. Bai, Y. Jiang, Cryo-EM structure of a fungal mitochondrial calcium uniporter, Nature 559 (2018) 570–574.
[33] C. Fan, M. Fan, B.J. Orlando, N.M. Fastman, J. Zhang, Y. Xu, M.G. Chambers, X. Xu, K. Perry, M. Liao, L. Feng, X-ray and cryo-EM structures of the mitochondrial calcium uniporter, Nature 559 (2018) 575–579.
[34] R. Baradaran, C. Wang, A.F. Siliciano, S.B. Long, Cryo-EM structures of fungal and metazoan mitochondrial calcium uniporters, Nature 559 (2018) 580–584.
[35] E. Carafoli, W.X. Balcavage, A.L. Lehninger, J.R. Mattoon, Ca^{2+} metabolism in yeast cells and mitochondria, Biochim. Biophys. Acta 205 (1970) 18–26.
[36] S. Manon, M. Guerin, Evidence for three different electrophoretic pathways in yeast mitochondria: ion specificity and inhibitor sensitivity, J. Bioenerg. Biomembr. 25 (1993) 671–678.
[37] D.M. Arduino, J. Wettmarshausen, H. Vais, P. Navas-Navarro, Y. Cheng, A. Leimpek, Z. Ma, A. Delrio-Lorenzo, A. Giordano, C. Garcia-Perez, G. Médard, B. Kuster, J. García-Sancho, D. Mokranjac, J.K. Foskett, M.T. Alonso, F. Perocchi, Systematic identification of MCU modulators by orthogonal interspecies chemical screening, Mol. Cell 67 (2017) 711–723.
[38] H. Qadota, I. Ishii, A. Fujiyama, Y. Ohya, Y. Anraku, RHO gene products, putative small GTP-binding proteins, are important for activation of the CAL1/CDC43 gene product, a protein geranylgeranyltransferase in Saccharomyces cerevisiae, Yeast 8 (1992) 735–741.
[39] A. Yamada, T. Yamamoto, Y. Yoshimura, S. Gouda, S. Kawashima, N. Yamazaki, K. Yamashita, M. Kataoka, T. Nagata, H. Terada, D.R. Pfeiffer, Y. Shinohara, Ca^{2+}-induced permeability transition can be observed even in yeast mitochondria under optimized experimental conditions, Biochim. Biophys. Acta 1787 (2009) 1486–1491.
[40] A. Yamada, T. Yamamoto, N. Yamazaki, K. Yamashita, M. Kataoka, T. Nagata, H. Terada, Y. Shinohara, Differential permeabilization effects of Ca^{2+} and valinomycin on the inner and outer mitochondrial membranes as revealed by proteomics analysis of proteins released from mitochondria, Mol. Cell. Proteomics 8 (2009) 1265–1277.
[41] T. Yamamoto, A. Yamada, M. Watanabe, Y. Yoshimura, N. Yamazaki, Y. Yoshimura, T. Yamauchi, M. Kataoka, T. Nagata, H. Terada, Y. Shinohara, VDAC1, having a shorter N-terminus than VDAC2 but showing the same migration in an SDS-polyacrylamide gel, is the predominant form expressed in mitochondria of various tissues, J. Proteome Res. 5 (2006) 3336–3344.
[42] A. Lupas, M. Van Dyke, J. Stock, Predicting coiled coils from protein sequences, Science 252 (1991) 1162–1164.
[43] J. Walshaw, D.N. Woolfson, Socket: a program for identifying and analysing coiled-coil motifs within protein structures, J. Mol. Biol. 307 (2001) 1427–1450.
[44] T.A. Smith, P.M. Steinert, D.A. Parry, Modeling effects of mutations in coiled-coil structures: case study using epidermolysis bullosa simplex mutations in segment 1a of K5/K14 intermediate filaments, Proteins 55 (2004) 1043–1052.
[45] C.L. Marolda, E.R. Haggerty, M. Lung, M.A. Valvano, Functional analysis of predicted coiled-coil regions in the Escherichia coli K-12 O-antigen polysaccharide chain length determinant Wzz, J. Bacteriol. 190 (2008) 2128–2137.
[46] V. Paupe, J. Prudent, E.P. Dassa, O.Z. Rendon, E.A. Shoubridge, CCDC90A (MCUR1) is a cytochrome c oxidase assembly factor and not a regulator of the mitochondrial calcium uniporter, Cell Metab. 21 (2015) 109–116.
[47] M.F. Tsai, C.B. Phillips, M. Ranaghan, C.W. Tsai, Y. Wu, C. Willliams, C. Miller, Dual functions of a small regulatory subunit in the mitochondrial calcium uniporter complex, Elife (2016) 5.
[48] N. Guex, M.C. Peitsch, T. Schwede, Automated comparative protein structure modeling with SWISS-MODEL and Swiss-PdbViewer: a historical perspective, Electrophoresis 30 Suppl 1 (2009) S162–S173.
[49] J. Marshall, D.V. Holberton, Sequence and structure of a new coiled coil protein from a microtubule bundle in Giardia, J. Mol. Biol. 231 (1993) 521–530.
[50] I. Iscla, R. Wray, P. Blount, On the structure of the N-terminal domain of the MscL channel: helical bundle or membrane interface, Biophys. J. 95 (2008) 2283–2291.
[51] T.A. Walton, D.C. Rees, Structure and stability of the C-terminal helical bundle of the E. coli mechanosensitive channel of large conductance, Protein Sci. 22 (2013) 1592–1601.
[52] K. Yoshimura, M. Sokabe, Mechanosensitivity of ion channels based on protein-lipid interactions, J. R. Soc. Interface 7 (Suppl. 3) (2010) S307–S320.
[53] Y. Wang, J. NX Nguyen, W. She, Y. Yang Zeng, X.C. Bai, Y. Jiang, Structural mechanism of EMRE-dependent gating of the human mitochondrial calcium uniporter, Cell 177 (2019) 1252–1261.